Dominant inflation of the Arctic Ocean's Beaufort Gyre in a warming climate

Check for updates

Qiang Wang [1,6] ✉, Qi Shu [2,3,6], Shizhu Wang[2,3], Xinyue Li [1], Sergey Danilov [1], Fangli Qiao [2,3], Zhenya Song [2,3], Fan Wang [4] & Thomas Jung [1,5]

The Arctic Ocean's Beaufort Gyre, the largest Arctic freshwater reservoir, plays a crucial role for climate and marine ecosystems. Understanding how it changes in a warming climate is therefore essential. Here, using high-resolution simulations and Coupled Model Intercomparison Project phase 6 data, we find that the Beaufort Gyre will increasingly accumulate freshwater, elevate sea level, and spin up its circulation as the climate warms. These changes, collectively referred to as inflation, are more pronounced in the Beaufort Gyre region than in other Arctic areas, amplifying the spatial asymmetry of the Arctic Ocean. The inflation is driven by increased surface freshwater fluxes and intensified surface stress from wind strengthening and sea ice decline. Current climate models tend to underestimate this inflation, which could be alleviated by high-resolution ocean models and improved atmospheric circulation simulations. The inflation of the Beaufort Gyre underscores its growing importance in a warming climate.

The Arctic Ocean, a critical component of Earth's climate system, is undergoing rapid changes[1–4]. Among various Arctic regions, the large, clockwise-rotating Beaufort Gyre in the Arctic Ocean's Canada Basin stands out as one of the most prominent features[5]. The Beaufort Gyre serves as a vast reservoir of freshwater, accumulating input from river runoff, precipitation, melting sea ice, and low-salinity water from the Pacific[6–9]. In the central Beaufort Gyre, surface salinity fell below 27 during the summer months in recent years[10,11], and the isohaline corresponding to the Arctic mean salinity of 34.8[12] is located at approximately 400 meters depth.

Arctic freshwater storage is crucial for upper ocean stratification, influencing ocean stability, vertical heat flux and thus sea ice melting[13–15]. Sea ice retreat can amplify Arctic warming and climate change[16]. Furthermore, the release of freshwater from the Beaufort Gyre into the North Atlantic can affect upper ocean stratification and wintertime deep convection in regions of dense water formation, thereby impacting the Atlantic Meridional Overturning Circulation (AMOC)[17–20], a key player in regulating global climate. Moreover, the gyre's ability to retain and release freshwater has strong implications for the Arctic Ocean's salinity and density gradients, influencing the broad circulation pattern in the Arctic Ocean[21]. Importantly, changes in the Beaufort Gyre circulation and stratification can also modify local concentration of dissolved oxygen and acidified water, with profound impacts on marine ecosystems[22,23].

During the past two decades, the Beaufort Gyre has experienced notable changes. These changes are marked by increases in the gyre's sea level and circulation strength[24], the volume of freshwater it retains[25–27], and mesoscale eddy activity[28], induced by factors such as sea ice decline and atmospheric circulation changes[29–32]. In particular, the amount of freshwater stored in the Beaufort Gyre reached an unprecedented high in the late 2010s[3,11,33,34]. Part of the anomalous freshwater from the Beaufort Gyre, released over the past few years, has accumulated in a buffer zone north of Greenland and the Canadian Arctic Archipelago[35]. As the Arctic continues to lose sea ice, the state of the Beaufort Gyre is expected to shift, potentially leading to substantial changes in the Arctic Ocean's physical and biogeochemical environment.

The Beaufort Gyre's importance for climate and marine ecosystems points to the need for a better understanding of how it will evolve in a warming climate. Predicting future ocean changes relies on coupled climate model projections, but simulating the Arctic Ocean and the Beaufort Gyre faces challenges. Current climate models often struggle with adequately representing salinity, temperature and stratification in the Arctic Ocean[36–39]. In particular, most Coupled Model Intercomparison Projects (CMIP) models exhibit a fresh bias in the Arctic halocline[37] and simulate an oversized Beaufort Gyre[38]. Ocean-sea ice model simulations forced by prescribed atmospheric reanalysis fields tend to have similar model biases[40,41]. It was

Fig. 1 | Mean states and future changes in fresh-water content (FWC), sea surface height (SSH) and surface geostrophic current (SGC) speeds in CMIP6 models. a–c Multi-model mean of FWC in 1981–2000 (a), 2081–2100 (b), and the difference between the two periods (c). d–f, the same as (a–c), but for SSH. g–i, the same as (a–c), but for SGC speeds.
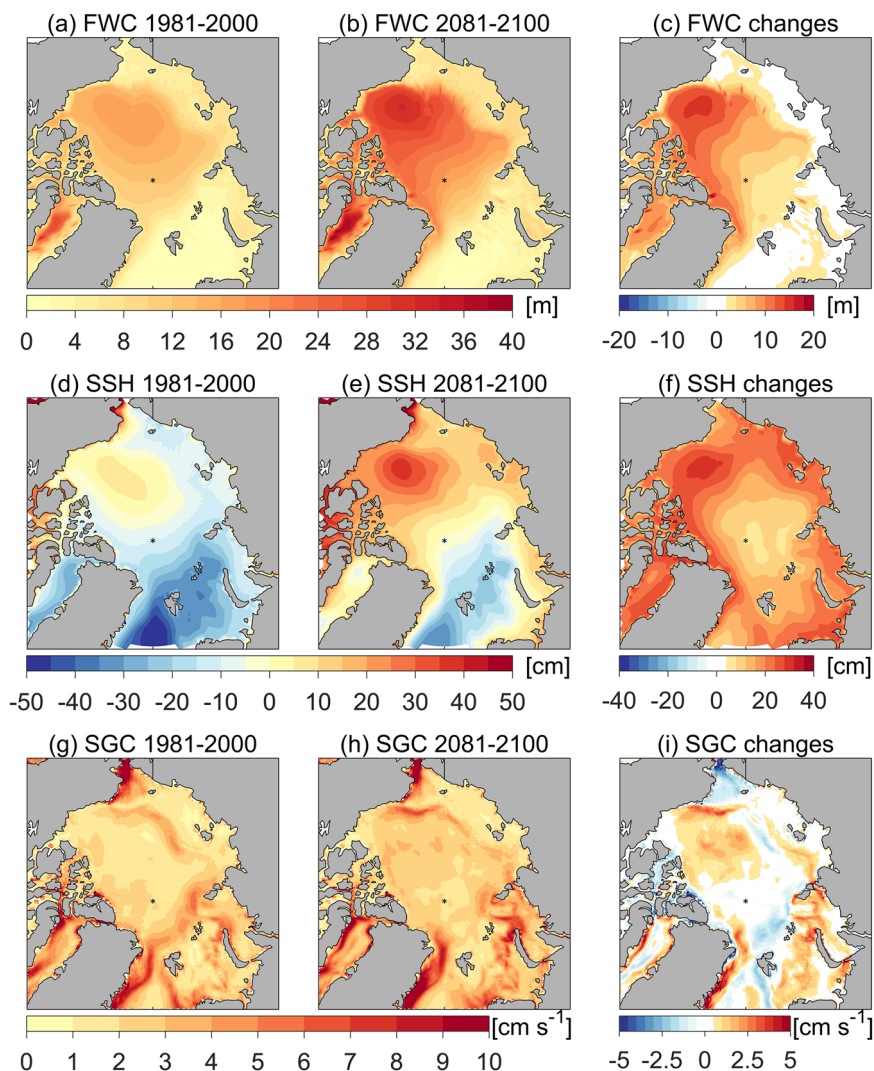
found that increasing horizontal resolution can help reduce model biases in simulated Arctic hydrography[42,43]. The recent 6th phase of CMIP (CMIP6) does not demonstrate clear improvements in simulating Arctic hydro-graphy compared with previous CMIP phases[37,41], likely due to the con-tinued use of coarse resolutions in most CMIP6 simulations. To improve the fidelity of future projections for the Arctic Ocean, efforts are needed to reduce model biases.

This paper utilizes CMIP6 dataset and dedicated high-resolution ocean-sea ice model simulations to elucidate future changes in Arctic Ocean freshwater and circulation (see Methods). We find that the Beaufort Gyre will increasingly accumulate freshwater in a warming climate, playing a dominant role in shaping the Arctic Ocean's circulation pattern. High-resolution simulations predict a much stronger spin-up of the Arctic Ocean circulation compared to CMIP6 models. Correcting a severe, common model bias in atmospheric circulation considerably intensifies projected increases in freshwater content, sea surface height, ocean current speeds, and eddy activity in the Beaufort Gyre region, further underscoring the dominance of the Beaufort Gyre inflation in future Arctic Ocean changes.

Results
Dominance of the Beaufort Gyre inflation in a warming climate
The CMIP6 historical simulations show a spatial concentration of fresh-water in the Canada Basin (Fig. 1a), which is associated with a dome in sea surface height (Fig. 1d), indicating an anticyclonic gyre circulation. How-ever, in comparison with the freshwater content (see Methods for definition) based on observed salinity climatology[44] and sea surface height and surface

geostrophic currents obtained from satellite observations[21,24], the simulated Beaufort Gyre exhibits an overly extensive area that encroaches into the Eurasian Basin (Fig. 2a, b and Supplementary Figs. S1, S2). The simulated salinity in individual CMIP6 models tends to show large biases relative to observations and there is a considerable spread among the models (Sup-plementary Fig. S3). As a result, the spread in simulated Beaufort Gyre freshwater content is also large (Fig. 3a).

The freshwater content is projected to increase in most areas of the Arctic deep basin (the Arctic area excluding continental shelf) in future warming climate, with the largest increase occurring in the Canada Basin (Fig. 1b, c). Compared to the period of 1981–2000, the freshwater content in the Beaufort Gyre region increases by an average of 12 m in the period of 2081–2100 according to the CMIP6 multi-model mean (MMM) (Fig. 3a, b), which corresponds to an increase of about 75%. This accumulation of freshwater in the Beaufort Gyre region clearly surpasses that of other Arctic regions, including the Eurasian and Makarov basins, as well as the shelf seas (Figs. 1c and 3b). As a result, the spatial asymmetry in Arctic freshwater distribution, with a concentration in the Canada Basin, will grow with climate warming.

In the future warming climate, the sea surface height in the Arctic deep basin is projected to increase, consistent with the increase in fresh-water content (Fig. 1e, f and Supplementary Fig. S4a). The sea surface height in this study refers to the dynamic sea level, which is relative to the global mean sea level and does not contain contributions from global total water mass changes. The Beaufort Gyre region is expected to experience the largest rise in sea surface height, with an average increase of about 24 cm during the period of 2081–2100 compared to the period of 1981–2000

(Figs. 1f, 3c, and d). The shallow shelf seas will also experience an increase in sea surface height, but this is not mainly attributable to ocean freshening (Fig. 1c, f). Instead, it is likely a result of increased water mass over the continental shelf due to deep-basin steric expansion, a phenomenon particularly pronounced in the Arctic[45,46]. The CMIP6 models predict strong freshening (Fig. 1c) and warming[4,37] trends in the Arctic deep basin, indicating the occurrence of deep-basin steric expansion, which can increase the water mass over surrounding continental shelf as suggested in previous studies[45,46]. Among the Siberian shelf seas, the East Siberian Sea shows the largest increase in mean sea surface height, with a magnitude slightly less than the mean increase in the Beaufort Gyre region (Fig. 3d).

Associated with the doming of the Beaufort Gyre, the surface geostrophic current in the gyre is expected to intensify in the future (Fig. 1h, i). The CMIP6 MMM indicates an increase of slightly more than 1 cm s^{-1} in the mean current speed between the two considered periods, larger than in other Arctic basins and shelf seas (Fig. 3e, f). The future changes in surface geostrophic current in the Beaufort Gyre region are not significantly correlated with changes in sea surface height across the CMIP6 models (Supplementary Fig. S4b), likely because the models simulate an oversized Beaufort Gyre, meaning the changes in the spatial gradients of sea surface height in the Beaufort Gyre region are not well represented. The mean surface geostrophic current speeds in shelf seas do not increase

Fig. 2 | Freshwater content (FWC) in the historical period. a Observational estimates based on PHC3[44]. **b** CMIP6 multi-model-mean (MMM). **c** FIO-ESM2.1 simulation. **d** FESOM2 high-resolution simulation without wind correction. **e** FESOM2 high-resolution simulation with wind correction. Model results are averaged over the period of 1981–2000.
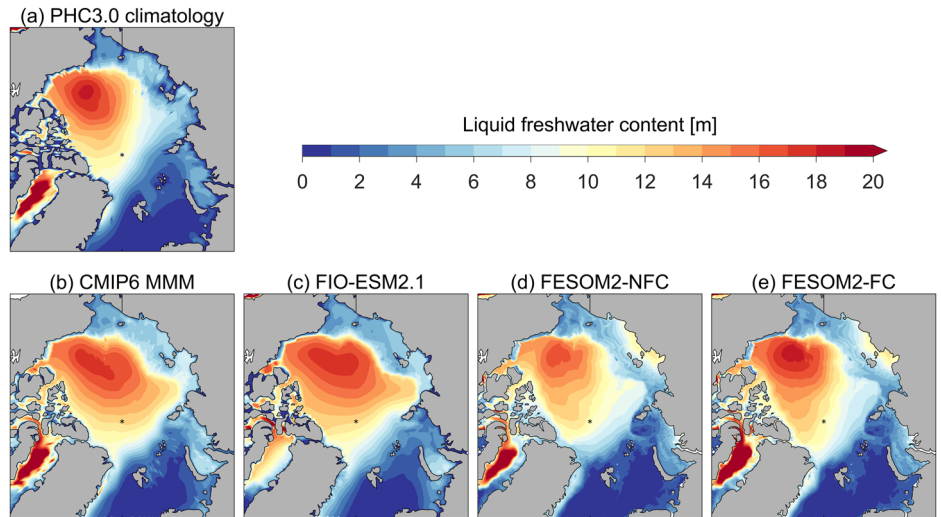
Fig. 3 | Dominance of the state change of the Beaufort Gyre in CMIP6 simulations. a Time series of freshwater content (FWC) in the Beaufort Gyre region. The thick solid line denotes the multi-model mean (MMM), the thin gray lines denote individual models, and the shading indicates model spreads (± 0.5 standard deviation). **b**, MMM changes of FWC between 1981–2000 and 2081–2100 in the Beaufort Gyre region in comparison with other Arctic regions. BG: Beaufort Gyre region (Canada Basin), MB: Makarov Basin, EB: Eurasian Basin, ESS: East Siberian Sea, LS: Laptev Sea, BKS: Barents-Kara seas. The inset depicts the Arctic regions analyzed in this study. The error bars indicate model spreads. **c–d** the same as (**a–b**), but for sea surface height (SSH). **e-f**, the same as (**a–b**), bur for surface geostrophic current (SGC) speeds.
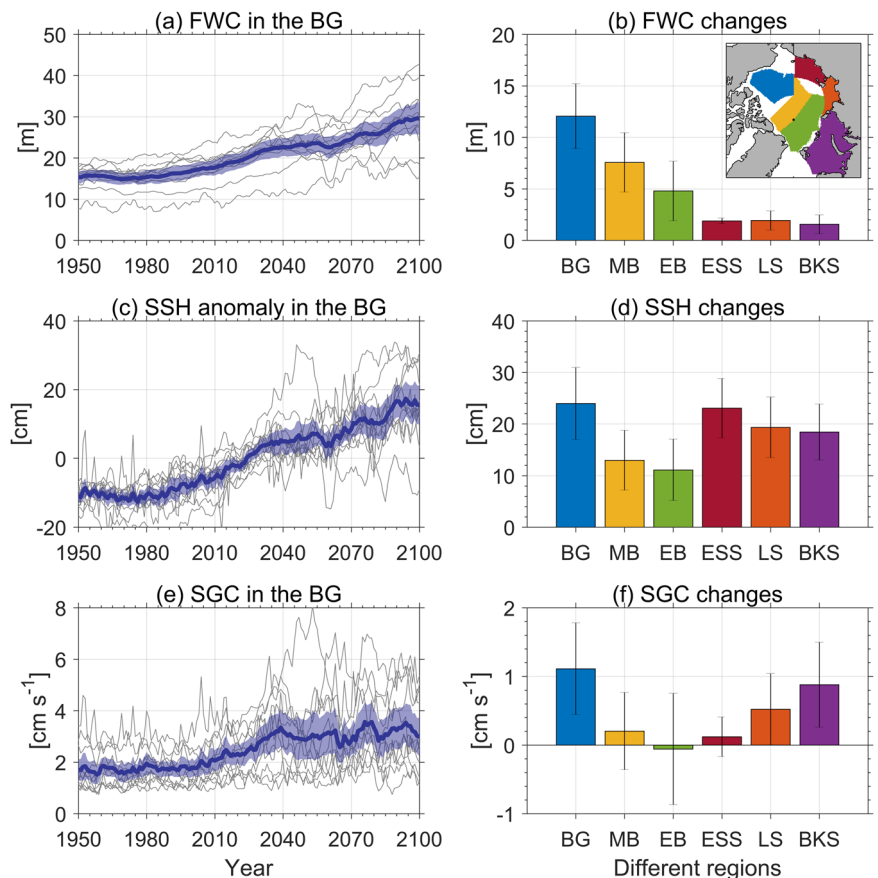
proportionally with the rise in sea surface height (Fig. 3d, f). This is because the relatively large spatial gradients of sea surface height — and thus the associated surface geostrophic currents—are confined to the continental slope areas (Fig. 1d–i).

The interannual variability of the freshwater content, sea surface height and surface geostrophic current in the Beaufort Gyre region is projected to increase in future warming climate (Fig. 4a–c), consistent with previous studies showing increased ocean response to winds when ocean surface stress and air-sea momentum transfer is enhanced by sea ice decline[47]. In contrast, the magnitudes of their seasonal cycles are projected to decrease (Fig. 4d–f), which can be explained by the weakening of the seasonal cycle of surface freshwater fluxes associated with diminishing sea ice seasonal melting and freezing.

Overall, the CMIP6 models demonstrate that the inflation of the Beaufort Gyre, including the increases in freshwater storage, sea surface height and geostrophic current speeds, will surpass those in other Arctic basins and shelf seas. The accumulation of freshwater in the Arctic Ocean is consistent with the projected rise in Arctic surface freshwater fluxes in a warming climate (Supplementary Fig. S5). Across the CMIP6 models, increases in Beaufort Gyre freshwater content are correlated with both the rise in surface freshwater fluxes and the decrease in surface stress curl (corresponding to increased Ekman convergence and downwelling) (Fig. 5a, b), two of the main factors contributing to Beaufort Gyre freshwater accumulation[3]. Transport by mesoscale eddies acts to counteract freshwater accumulation in the Beaufort Gyre[48,49]. The correlation coefficients between changes in freshwater content and changes in surface freshwater fluxes and surface stress curl are not very high (Fig. 5a, b), suggesting that the implementation of eddy parameterization, which varies across CMIP6 models, has considerable impacts on simulated freshwater content.

The increase in ocean surface stress in the Beaufort Gyre region correlates more strongly with rising wind speeds than with decreasing sea ice cover across the CMIP6 models (Fig. 5c, d). However, wind speeds in the Beaufort Gyre region are projected to increase by approximately 12% from 1981–2000 to 2081–2100 in the CMIP6 MMM, while ocean surface stress is projected to increase by about 48% over the same period, suggesting that sea ice decline plays an important role in amplifying ocean surface stress. This will be further demonstrated through the following sensitivity simulations.

Stronger ocean spin-up in high-resolution simulations

We performed a high-resolution FESOM2 simulation forced by atmospheric fields derived from a coupled climate model, which covers both the historical period and future projection (see Methods). This high-resolution simulation demonstrates a dominance of Beaufort Gyre inflation in the Arctic Ocean, supporting the main conclusions based on CMIP6 models (Figs. 6 and 7). Employing high resolution considerably improves the representation of the salinity vertical profile (Supplementary Fig. S3) and the spatial pattern of the Beaufort Gyre (Fig. 2). Our results indicate that, despite larger biases in the simulated mean state of salinity in individual CMIP6 models, their MMM changes in freshwater content and sea surface height averaged in the Canada Basin are similar to our high-resolution simulation (Fig. 6a, b).

The future increase in surface geostrophic current speeds is notably greater in the high-resolution simulation compared to the CMIP6 models (Fig. 6c), which is apparent in most areas of the Arctic Ocean (Figs. 1i and 7c). The discrepancy in the Beaufort Gyre region is linked to the larger spatial gradients in freshwater content and sea surface height in the Canada Basin captured by the high-resolution simulation (Supplementary Fig. S6). Furthermore, the high-resolution simulation is eddy-permitting. The eddy
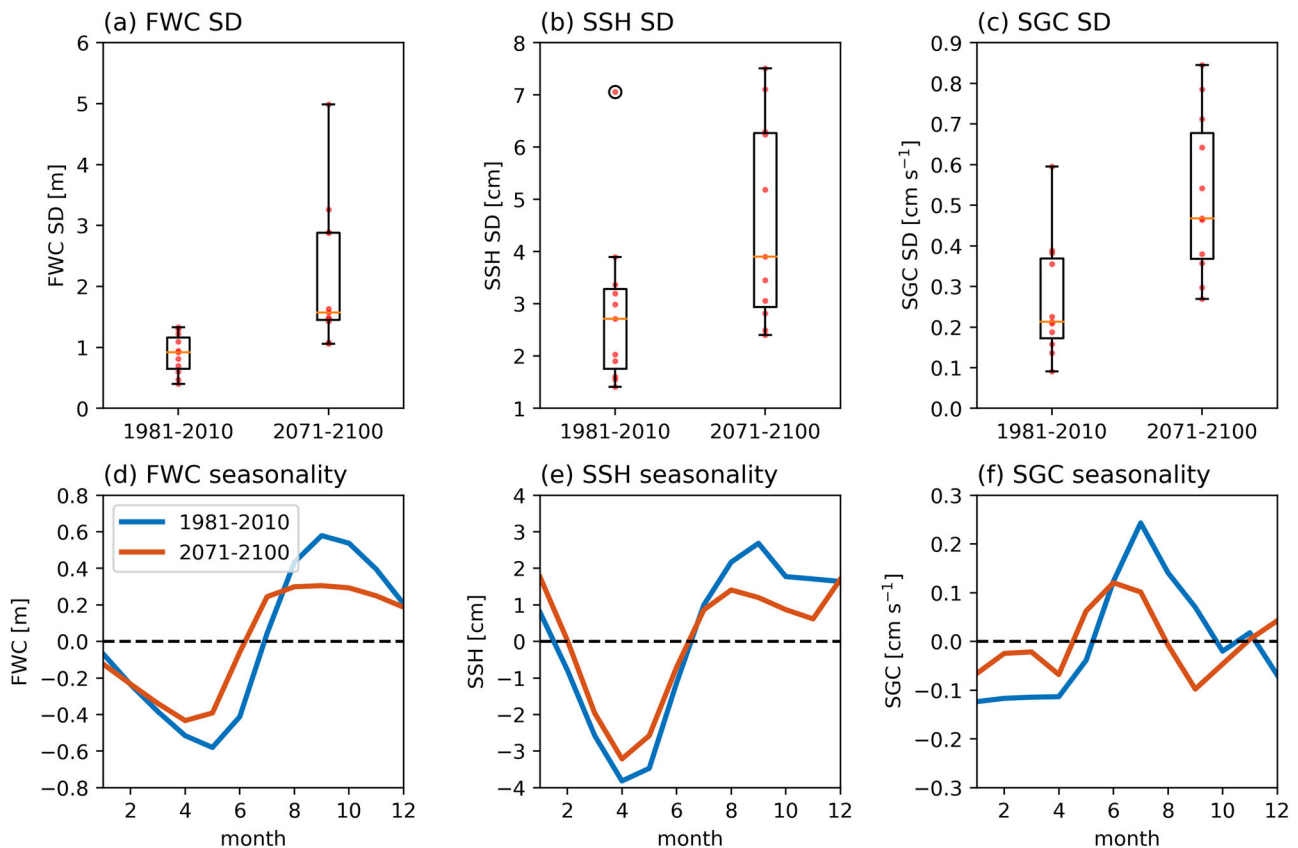

Fig. 4 | Interannual and seasonal variability in CMIP6 simulations. a–c The standard deviation (SD) of annual mean (**a**) freshwater content (FWC), (**b**) sea surface height (SSH) and (**c**) surface geostrophic current (SGC) speeds in the Beaufort Gyre. The SD was calculated after detrending. Red marks in the boxes indicate the median and the bottom and top edges of the boxes indicate the 25th percentile and 75th percentile, respectively. The black vertical lines extend to the most extreme data points not considered outliers. The black circle denotes outliers. Individual models are indicated by red dots. **d–f**, Seasonal variability of (**a**) FWC, (**b**) SSH and (**c**) SGC speeds in the Beaufort Gyre. Annual means are subtracted to obtain seasonal cycles.

Fig. 5 | Correlation relationship across CMIP6 models. a Correlation between changes in Beaufort Gyre freshwater content (FWC) and Arctic surface freshwater flux (SFF). **b** Correlation between changes in Beaufort Gyre FWC and surface stress curl (SSC). **c** Correlation between changes in Beaufort Gyre surface stress and near-surface wind speeds. **d** Correlation between changes in Beaufort Gyre surface stress and sea ice extent (SIE). The changes are the differences between 2081–2100 and 1981–2000.
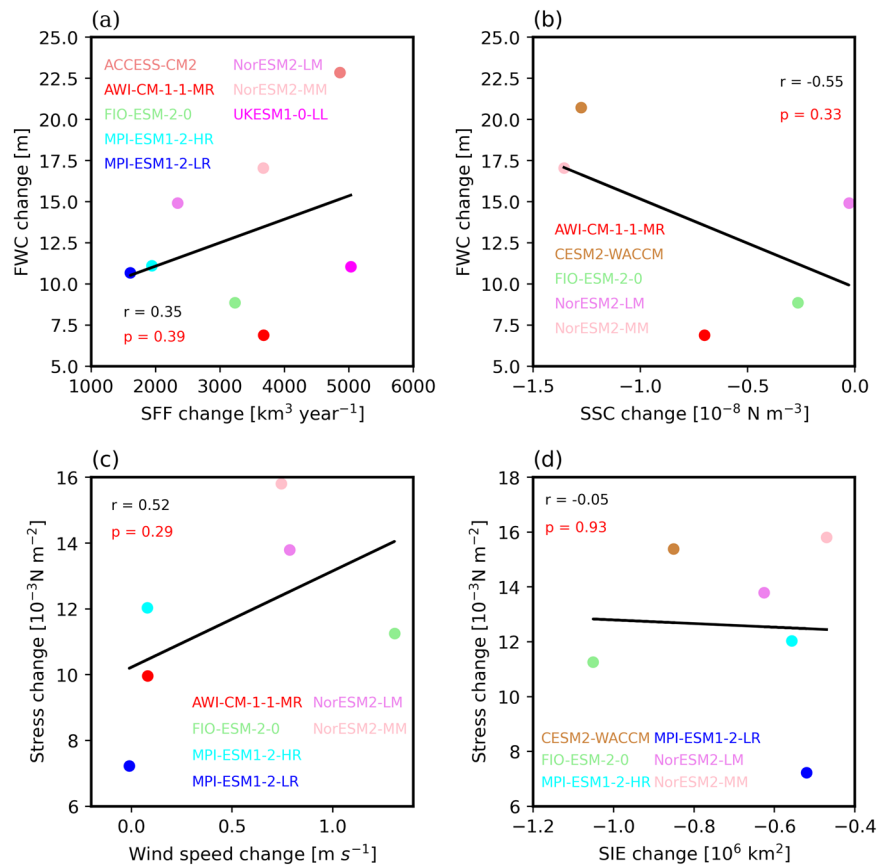
kinetic energy (EKE) in the Beaufort Gyre region is relatively low in the historical period due to sea ice dissipation, while it is projected to increase with sea ice decline under a warming climate (Supplementary Fig. S7a,c)[50]. Thus, the varying surface geostrophic currents associated with enhanced eddy activity also contribute to the increased current speeds in the high-resolution simulation. The current speeds in the Beaufort Gyre region, calculated from monthly mean sea surface height, are 5.3 cm s^{-1} larger in 2081–2100 than in 1981–2000 (Fig. 6c). This increase is much larger than the simulated increase of about 1 cm s^{-1} in the CMIP6 MMM.

In addition to the basin-wide ocean spin-up under a warming climate (Fig. 6c), the high-resolution simulation projects a future strengthening of Arctic boundary currents along the continental slopes (Fig. 7c). This trend is substantially weaker in the CMIP6 models (Fig. 1i).

Greater-than-projected Beaufort Gyre inflation

The Beaufort Gyre is driven by the Arctic high-pressure system centered over the Canada Basin, known as the Beaufort High (Fig. 8a). In the CMIP6 models, the simulated Beaufort High during the historical period has a magnitude similar to observations, but its center is displaced toward the Eurasian sector (Fig. 8b), with a negative bias in sea level pressure in the western Arctic and a positive bias in the eastern Arctic (Fig. 8c). In the future warming climate, the Arctic sea level pressure is expected to decrease (Fig. 8b, d). In most CMIP6 models, the locations of their Beaufort High center in both the historical period and future scenarios remain closer to the central Arctic than observed (Supplementary Figs. S8 and S9). Considering different atmospheric reanalysis products and different historical periods, the sea level pressure biases in CMIP6 models remain similar (Supplementary Fig. S10). Assuming the models maintain the same biases in the future, we subtract the biases from the sea level pressure over time. This correction results in a stronger Beaufort High with its center repositioned over the Canada Basin, rather than the central Arctic (Fig. 8e). The coupled climate model FIO-ESM2.1, from which we derived atmospheric fields to drive FESOM2 simulations, shows a bias pattern similar to CMIP6 models (Fig. 8f–i).

We corrected the wind forcing for the entire period by subtracting the wind biases averaged over the historical period and used both the uncorrected (FESOM2 NFC) and corrected (FESOM2 FC) winds to drive the high-resolution FESOM2 simulations (see Methods). By comparing the two simulations we can understand how the wind biases influence the simulated changes in the Beaufort Gyre.

The corrected winds considerably increase the accumulation of freshwater in the Beaufort Gyre region (Fig. 7a, d), which can be explained by enhanced ocean surface stress and thus Ekman transport toward the Canada Basin (Supplementary Figs. S11,S12). The increase of the freshwater content in the Beaufort Gyre from 1981–2000 to 2081–2100 is 32% larger with the wind correction (Fig. 9a and Supplementary Fig. S13). Correspondingly, the future increase in sea surface height in the Beaufort Gyre is 45% larger with the wind correction (Figs. 7b, e and 9b). The surface geostrophic current speeds in the Beaufort Gyre region are also intensified with the wind correction (Fig. 7c, f), reaching a future increase of about 7 cm s^{-1}, which is 27% greater than the case without wind correction (Fig. 9c). Comparing the two high-resolution simulations, it is evident that the wind biases lead to an underestimation of the dominance of the Beaufort Gyre inflation in shaping the Arctic Ocean changes (Figs. 6 and 7). Since the same wind correction was applied throughout the simulation, the fact that the simulation with wind correction shows a larger inflation of the Beaufort Gyre in the future warming climate reveals the role of sea ice decline in increasing ocean surface stress, and consequently, Ekman convergence toward the Beaufort Gyre region (Supplementary Figs. S11,S12).

Due to greater freshwater accumulation, the increase of available potential energy (APE) in the upper 300 m of the Beaufort Gyre from 1981–2000 to 2081–2100 is 34% larger with the wind correction (Fig. 9d). With the wind correction, the mean kinetic energy (MKE) in the upper 300 m of the Beaufort Gyre is projected to increase by 70% more (Fig. 9e). Owing to the greater increase in freshwater content and APE, the increase in Beaufort Gyre eddy kinetic energy (EKE) is 61% larger (Fig. 9f). While correcting winds does not obviously affect the EKE in the historical period, it
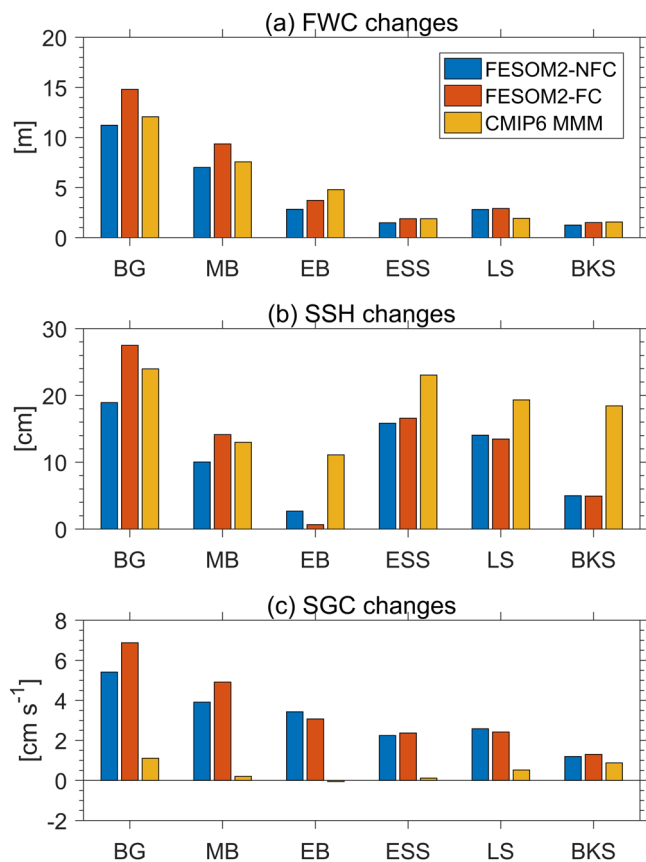
Fig. 6 | **Dominance of the state change of the Beaufort Gyre in high-resolution and CMIP6 simulations. a** Changes of freshwater content (FWC) between 1981–2000 and 2081–2100 in the Beaufort Gyre region in comparison with other Arctic regions. BG: Beaufort Gyre region (Canada Basin), MB: Makarov Basin, EB: Eurasian Basin, ESS: East Siberian Sea, LS: Laptev Sea, BKS: Barents-Kara seas. These regions are depicted in Fig. 3b. **b** the same as (**a**), but for sea surface height (SSH). **c** the same as (**a**), but for surface geostrophic current (SGC) speeds.

has a strong impact in the future warming climate (Supplementary Fig. S7), highlighting the role of sea ice decline in amplifying the effects of wind anomalies. The wind correction also strengthens the projected increase in freshwater content, sea surface height and surface geostrophic current speeds in the Makarov Basin, although the strengthening is less pronounced than in the Beaufort Gyre region (Fig. 6).

Discussion

The Beaufort Gyre regulates the Arctic Ocean's physical and biogeochemical environment and influences deep water formation in the subpolar North Atlantic[3,11,22]. Understanding and predicting its changes in a warming climate is therefore crucial. Using results from CMIP6 coupled climate models and dedicated high-resolution simulations, we find that the Beaufort Gyre will accumulate more freshwater, experience a rise in sea level, and undergo intensified circulation as the climate continues to warm. This inflation is more pronounced than in other Arctic basins and shelf seas, causing the Beaufort Gyre to become a more dominant feature of the Arctic Ocean. The growing asymmetry in the spatial distribution of Arctic Ocean freshwater, with an increasing concentration in the Canada Basin, implies rising importance of the Beaufort Gyre. While the Beaufort Gyre will experience dominant inflation, our high-resolution simulations also indicate a widespread spin-up of ocean circulation throughout the Arctic.

Atmospheric cyclone (low-pressure system) activity in the Arctic has shown an increasing trend over the last few decades[51] and is projected to continue increasing in the future[52]. An observed increase in the intrusion of

cyclones from lower latitudes into the Arctic has tended to weaken the atmospheric Beaufort High[53,54]. In addition, the Arctic is also warming two to three times faster than the global average[16,55]. Consistent with the effects of cyclones and the generation of thermal lows, there will be a reduction in Arctic sea level pressure in a warming climate (Fig. 8 and Supplementary Fig. S14). However, the Arctic winds will rather strengthen (Fig. 5c) due to weakened atmospheric stability[56,57]. The resulting increase in ocean surface stress and the projected increase in surface freshwater fluxes together will lead to Beaufort Gyre inflation.

Across the analyzed CMIP6 models, the projected increase in ocean surface stress in the Beaufort Gyre region is not correlated with the decrease in sea ice extent (Fig. 5d). However, this does not imply that the decline in sea ice does not contribute to the simulated increases in ocean surface stress and freshwater accumulation. First, ocean surface stress is influenced by ocean surface currents in the presence of seasonal sea ice. Consequently, uncertainties in the simulated freshwater content associated with factors such as eddy and mixing parameterizations, may weaken the correlation between changes in ocean surface stress and sea ice extent across the models. Second, dedicated modeling studies, in which winds remain the same while Arctic sea ice cover is reduced by increasing Arctic air temperature, have shown that sea ice decline considerably enhances ocean surface stress and Ekman transport[58]. Similarly, the decline of sea ice over the past two decades has been found to play a key role in the spatial distribution of freshwater in the Arctic Ocean by increasing ocean surface stress[33]. Third, as shown by our high-resolution simulations, although the same wind anomaly is added to the wind forcing throughout the simulations, the differences in the ocean are much more pronounced in the future than in the current climate (Fig. 9). This clearly demonstrates the effects of sea ice decline in amplifying ocean surface stress.

Eddies act to counteract increases in freshwater content in the Beaufort Gyre[28,48,49]. CMIP6 models, which have very coarse resolution and parameterized eddy effects, exhibit a large spread in the simulated Arctic Ocean hydrography and freshwater content as shown in this work (Figs. 3 and 5) and previous studies[36–38,59]. The misrepresentation of the spatial extent of the Beaufort Gyre in these coarse-resolution models leads to an underestimation of the projected increase in Beaufort Gyre circulation, potentially causing biases in ocean-ice stress. The spatial extent of the Beaufort Gyre is more realistically simulated in the high-resolution simulations. They predict much greater increases in surface geostrophic current speeds in the Beaufort Gyre and along Arctic continental slopes than CMIP6 models. Although we cannot exclude possible uncertainties in projected ocean changes associated with uncertainties in the global atmospheric fields used to drive our high-resolution simulations, our study addresses the benefit of using high-resolution ocean models. It remains to see how further increases in model resolution, reaching a scale of eddy-rich ocean, might influence the quantitative representation of future freshwater content in the Beaufort Gyre region.

Present climate models commonly exhibit a bias in simulating the atmospheric Beaufort High, extending it too far into the Eurasian Arctic (Fig. 8). This bias tends to lower the freshwater content in the Canada Basin and the strength of the Beaufort Gyre. Notably, the impact of this bias on the ocean increases with sea ice decline. This also highlights the role of sea ice decline in enhancing ocean surface stress and air-sea momentum transfer under a warming climate. Our results suggest that the dominance of the Beaufort Gyre inflation is likely underestimated in CMIP6 models. Our high-resolution simulations indicate that correcting the wind bias also intensifies the projected increase in Beaufort Gyre eddy activity in a warming climate.

The Beaufort Gyre is a prominent feature of the Arctic Ocean in the present climate. Its strong inflation in a warming climate implies an increasing role in modulating the distribution of freshwater and chemical tracers in both the Arctic Ocean and the subpolar North Atlantic, with greater impacts on climate and marine ecosystems. Sustained observations and improved climate models are important for better understanding and predicting the evolving role of the Beaufort Gyre.

Fig. 7 | Future changes in freshwater content (FWC), sea surface height (SSH) and surface geostrophic current (SGC) speeds in high-resolution simulations. a–c Changes in (**a**) FWC, (**b**) SSH and (**c**) SGC between 1981–2000 and 2081–2100 in the simulation without wind corrections. **d–f**, The same as (**a–c**), but for the simulation with wind corrections. In the latter simulation, wind biases associated with the sea level pressure biases depicted in Fig. 8g are subtracted from the applied wind forcing.
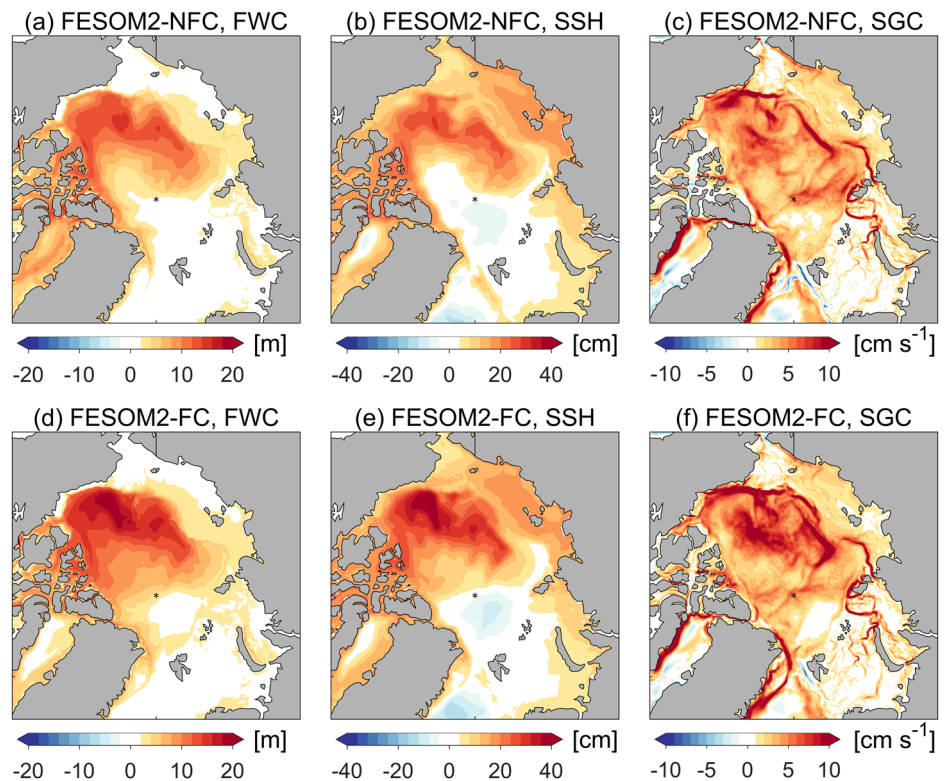
Methods
CMIP6 dataset
We used historical and projection simulations from 39 CMIP6 coupled climate models (Table S1). The employed CMIP6 simulations cover the periods 1950–2014 for historical experiments and 2015–2100 for projection experiments. The projections used in this study are based on the SSP585 scenario, which represents a pathway of rapid, fossil-fueled development with an effective radiative forcing of 8.5 Wm^{-2} in 2100[60]. By using this scenario, the time series of the analyzed variables illustrate their evolution in line with the trajectory of climate warming, from the current climate to a world with 4 °C of global temperature increase[61]. We analyzed the following diagnostics from these CMIP6 models: freshwater content (FWC, equation 1), sea surface height, surface geostrophic current speeds, salinity profiles, surface freshwater fluxes (including runoff, precipitation, evaporation and fluxes associated with sea ice thermodynamic processes), sea level pressure, sea ice extent, ocean surface stress, surface stress curl and near-surface wind speeds. Not all the required variables are available in every CMIP6 model for analyzing these diagnostics (Table S1). In particular, the number of models providing sea surface height (dynamic sea level), ocean surface stress and grid information allowing to calculate surface stress curl is limited. For consistency, we used models that provide both three-dimensional salinity and sea surface height data when these two variables are linked or compared, including Figs. 1, 2, 3. Due to the relatively small size of the ensemble, the fingerprint of individual models' internal variability is not fully eliminated in the MMM, as shown in Fig. 3a, c, e.

Our evaluation of CMIP6 MMM results reveals that the simulated Arctic precipitation minus evaporation in the historical period closely matches reanalysis and synthesized climatology, while river runoff is likely underestimated (Supplementary Fig. S5a). The simulated changes in Arctic sea ice extent are in good agreement with satellite observations (Supplementary Fig. S5b). The models tend to have fresh biases in the halocline and saline biases near the surface (Supplementary Fig. S3). The spatial extent of the Beaufort Gyre is considerably overestimated (Fig. 2 and Supplementary Figs. S1,S2). The large ocean biases in CMIP6 models highlight the need for high-resolution simulations, which are used in this study. Additionally, CMIP6 models show a common bias in Arctic sea level pressure, with the

center of the Beaufort High displaced toward the Eurasian Basin (Fig. 8 and Supplementary Figs. S8,S9). This motivates the correction of the wind bias in our high-resolution simulations. Details are provided in the sections below.

It is important to note that climate models do not necessarily reproduce observed variability in the historical period. For example, if the strengthening of the anticyclonic winds over the Canada Basin during the last two decades[3] is absent in a coupled climate simulation, we would not expect the simulated freshwater content in the Beaufort Gyre to increase as much as observed (Supplementary Fig. S13). This discrepancy also helps explain why the simulated sea surface height and surface geostrophic currents are weaker than those from recent satellite observations (Supplementary Figs. S1,S2).

High-resolution simulations
We performed high-resolution simulations using the Finite volumE Sea ice-Ocean Model (FESOM2)[62,63]. FESOM2 is a global general circulation ocean model that employs unstructured meshes, allowing for variable horizontal resolutions and thus enabling efficient simulations.

The model configuration used in this study has a horizontal resolution of 4.5 km in the Arctic Ocean, decreasing to about 24 km in the subpolar region and 1° in most other parts of the global ocean. The resolution is also slightly increased to 1/3° in the equatorial belt and along coastlines. The mesh consists of 47 z-levels, with 5 m vertical spacing at the surface, which coarsens with depth. Eddy diffusivity is scaled with local horizontal resolution. In the Arctic region, the resolution is eddy-permitting, so parameterization for mesoscale eddies is switched off. This model setup was described and evaluated within the framework of Ocean Model Intercomparison Project phase 2 (OMIP2)[43]. When forced by atmospheric reanalysis fields, it demonstrates good performance in reproducing the observed mean state and temporal changes in the Arctic Ocean, including key parameters such as salinity, temperature, mixed layer depth, halocline depth, freshwater content and Arctic gateways transports[43].

The surface forcing used to drive FESOM2 is derived from the output of the coupled climate model FIO-ESM v2.1[64], an improved version of FIO-ESM v2.0, which participated in CMIP6[65]. FIO-ESM v2.0 demonstrated good skills in simulating atmospheric fields, ranking in the top two across 14 CORDEX (COordinated Regional Downscaling EXperiment) domains,
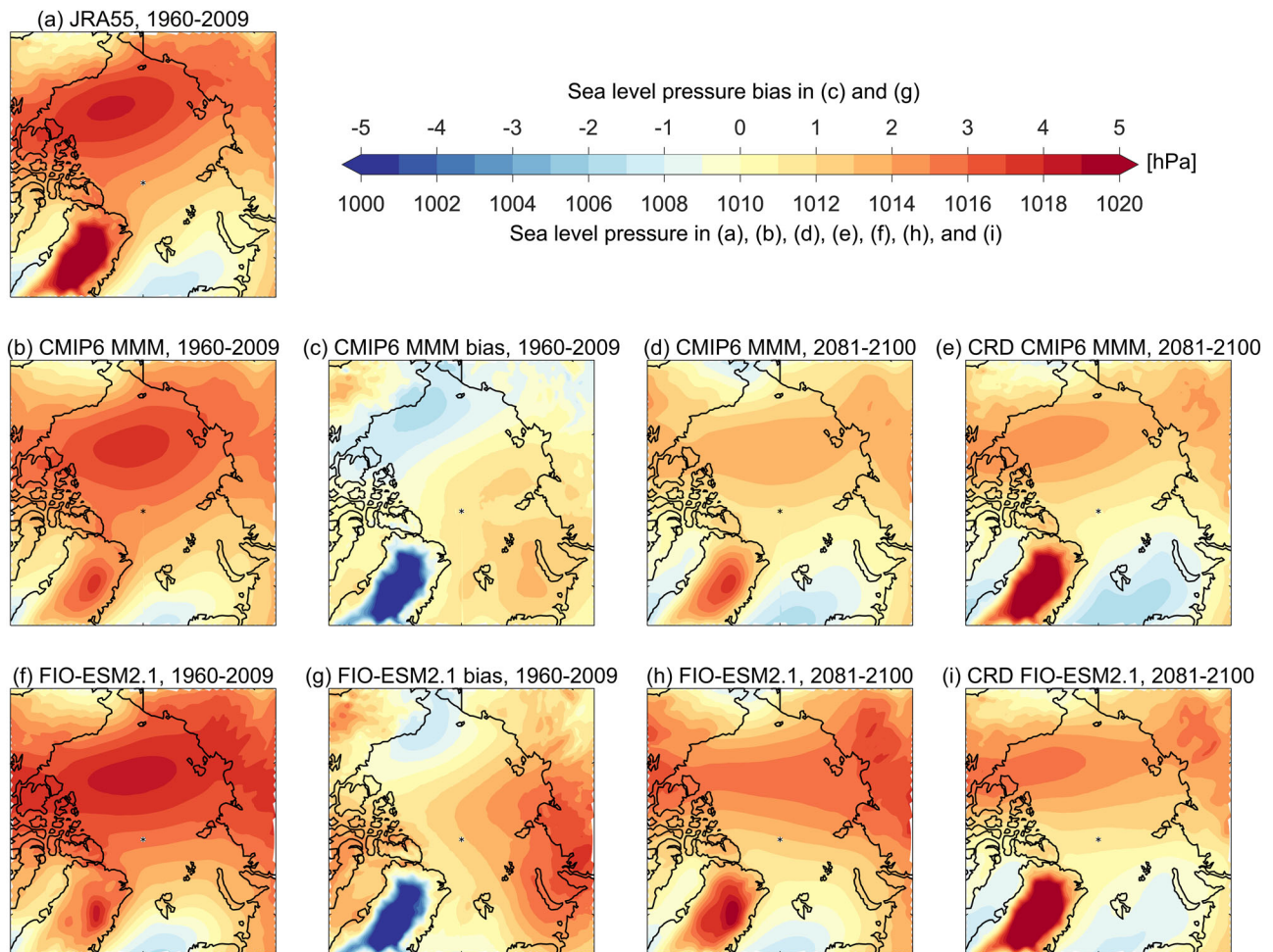
Fig. 8 | Atmospheric circulation bias in climate model simulations. a Sea level pressure (SLP) in atmosphere reanalysis JRA55-do averaged over the period of 1960–2009. **b** CMIP6 multi-model mean (MMM) SLP averaged over the period of 1960–2009. **c**, SLP bias of CMIP6 MMM averaged over the period of 1960–2009.

d, CMIP6 MMM SLP averaged over the period of 2081–2100. **e** Corrected (CRD) CMIP6 MMM SLP averaged over the period of 2081–2100. **f–i**, the same as (**b–e**), but for the SLP from the FIO-ESM2.1 simulation.

including the Arctic region[66]. The update to FIO-ESM v2.1 aims to further improve sea ice simulations by upgrading its sea ice component model and improving ice-ocean heat exchange parameterization[64]. The atmospheric fields and river runoff derived from FIO-ESM v2.1 cover the historical period (1900–2014) and the SSP585 future scenario (2015–2100). These fields include near-surface winds, air temperature, specific humidity, downward shortwave radiation, downward longwave radiation, rainfall, and snowfall, with a spatial resolution of $1.25° \times 0.9°$ and a temporal resolution of three hours.

The FESOM2 simulations are initialized using observed temperature and salinity from Polar Science Center Hydrographic Climatology version 3 (PHC3)[44]. The simulations cover the entire period from 1900 to 2100. Compared to observations, FESOM2 historical simulations provide a more accurate representation of the salinity vertical profile (Supplementary Fig. S3) and the spatial pattern of the Beaufort Gyre than CMIP6 models and FIO-ESM v2.1 (Fig. 2 and Supplementary Figs. S1,S2). Therefore, we expect that the FESOM2 simulations offer more reliable predictions of future Arctic Ocean changes upon the reliability of the applied surface forcing.

Forcing correction
We found that nearly all CMIP6 models exhibit a common bias in simulated sea level pressure in the historical period, with the Beaufort High excessively extending into the Eurasian Arctic compared to JRA55-do[67] reanalysis data (Supplementary Fig. S8). The CMIP6 MMM sea level pressure shows a positive bias in the eastern Arctic and a negative bias in

the western Arctic (Fig. 8b, c). FIO-ESM2.1 displays a similar bias (Fig. 8f, g). Using different reanalysis products for different periods, the CMIP6 models' bias is found to be similar (Supplementary Fig. S10). Although the exact cause of this common model bias is unknown, it is reasonable to assume that climate models tend to have similar biases in their projection simulations. Indeed, the projected Beaufort High in future warming climate shows a spatial displacement similar to the historical simulations despite an overall reduction in Arctic sea level pressure (Fig. 8b, d and Supplementary Fig. S9). If we subtract the sea level pressure bias of the historical simulations from the sea level pressure of the future projections, we recover the canonical pattern of sea level pressure, with the center of the Beaufort High located over the Canada Basin (Fig. 8e, i). If we apply this correction to the sea level pressure of the historical simulations (Fig. 8b, f), by definition, the resultant sea level pressure is exactly the same as the reanalysis data used to calculate the bias.

Sea level pressure is used in Fig. 8 to illustrate the bias in the atmospheric circulation and the concept of forcing correction, but it is the winds, not sea level pressure, that are used to drive model simulations. To assess the impacts of this common bias on the simulated Arctic Ocean, we corrected the winds derived from FIO-ESM2.1 and performed another FESOM2 simulation. First, we calculated the temporal-mean biases of the zonal and meridional winds relative to the JRA55-do atmospheric reanalysis[67] averaged over the period 1960–2009. The biases were calculated for each 3-hourly record separately. Then, these 3-hourly biases were
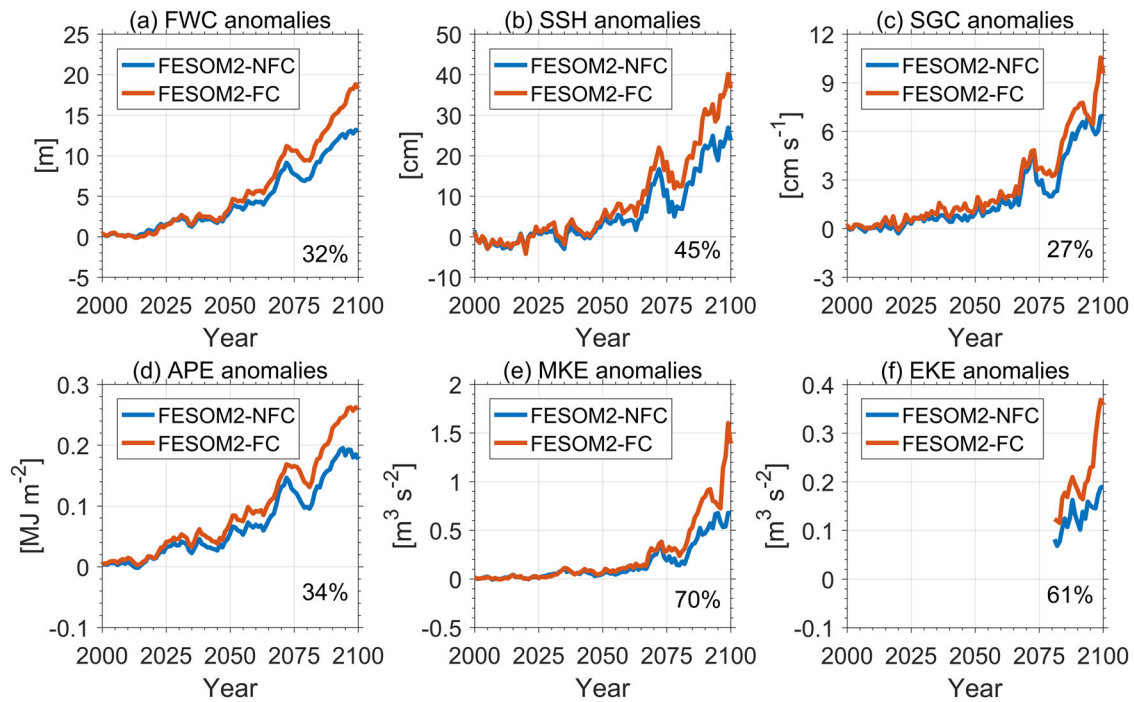
Fig. 9 | Underestimated state change of the Beaufort Gyre due to bias in atmospheric circulation simulations. a Anomaly of Beaufort Gyre freshwater content (FWC) relative to the 1981-2000 mean. **b-f**, the same as (**a**), but for (**b**) sea surface height (SSH), (**c**) surface geostrophic current (SGC) speeds, (**d**) upper 300 m available potential energy (APE), (**e**) upper 300 m mean kinetic energy (MKE), and (**f**) upper 300 m eddy kinetic energy (EKE) in the Beaufort Gyre region. The blue lines denote the results of the high-resolution simulation without wind corrections, and the red lines denote those with wind corrections. The percentages of the differences between the two simulations averaged over 2081–2100 are shown in each panel. The EKE data are only saved from the simulations for some years.

subtracted from the 3-hourly winds for the entire period (1900–2100). This forcing correction does not change the interannual variability and trend of winds. Comparing the FESOM2 simulation with forcing correction (FC) and the one without forcing correction (NFC) reveals the impacts of the common bias in atmospheric circulation. As shown in the main text, we find that the inflation of the Beaufort Gyre is likely underestimated in CMIP6 simulations due to this atmospheric circulation bias.

Analysis of ocean model data

The FWC in a water column is defined as follows:

$$\mathrm{FWC} = \int_D^{\mathrm{surface}} (S_{\mathrm{ref}} - S)/S_{\mathrm{ref}}\, \mathrm{d}z, \qquad (1)$$

where S denotes ocean salinity, S_{ref} the reference salinity, D the depth where ocean salinity is equal to the reference salinity, and z the vertical coordinate. The reference salinity is set to 34.8, the mean salinity of the Arctic Ocean[12]. The FWC in a column refers to the amount of pure water that can be extracted so that the mean salinity of the column equals the reference salinity. As changes in steric height (that is, changes in sea level due to ocean density changes associated with temperature and salinity changes) in the Arctic deep basin are mainly determined by salinity changes, FWC is directly correlated with sea surface height. In practice, this relationship allows FWC changes to be derived using satellite-observed sea surface height changes[3,24–26]. To keep the consistency, we used CMIP6 models that provide both salinity and sea surface height data for both historical and projection simulations for our analysis of FWC and sea surface height.

The available potential energy (APE) in the upper 300 m is defined following previous studies[68]:

$$\mathrm{APE} = \int_{300\mathrm{m}}^{\mathrm{surface}} g(\rho - \rho_{\mathrm{ref}}) z\, \mathrm{d}z, \qquad (2)$$

where g is the gravity acceleration, ρ is potential density, and ρ_{ref} is the potential density at 300 m depth. An increase in FWC is expected to increase APE, thus increasing mesoscale eddy activity.

We use the Reynolds averaging method to split the total kinetic energy (TKE) into mean kinetic energy (MKE) and eddy kinetic energy (EKE) components. MKE represents kinetic energy associated with the mean flow, while EKE represents kinetic energy associated with turbulent and eddy fluctuations in the flow. We decompose ocean velocity to a time mean component (indicated by overbars) and an eddy component (indicated by primes), $\mathbf{u} = (u, v) = (\bar{u} + u', \bar{v} + v')$. MKE and EKE are calculated as follows:

$$\mathrm{MKE} = \frac{1}{2}(\overline{u}^2 + \overline{v}^2), \qquad (3)$$

$$\mathrm{EKE} = \mathrm{TKE} - \mathrm{MKE} = \frac{1}{2}(\overline{u^2} + \overline{v^2}) - \frac{1}{2}(\overline{u}^2 + \overline{v}^2) = \frac{1}{2}(\overline{u'^2} + \overline{v'^2}). \qquad (4)$$

Here, $\bar{u}, \bar{v}, \overline{u^2}$ and $\overline{v^2}$ are monthly means from the model output. $\overline{u^2}, \overline{v^2}$ are saved only for the periods of 1981–2000 and 2081–2100 in the FESOM2 simulations, so EKE is available for these periods.

Observational and reanalysis datasets

The following datasets are used in this study to evaluate model results: the PHC3 gridded salinity data based on in-situ observations[44], sea surface height and surface geostrophic currents from satellite measurements[21,24], time series of freshwater content in the Beaufort Gyre derived from in-situ salinity observations[3,11], synthesized surface freshwater fluxes[8], river runoff estimates based on observations[69], precipitation and evaporation data from the ERA-Interim reanalysis[70], sea level pressure from the JRA55-do[67], ERA5[71], and MERRA2[72] reanalysis products, and sea ice extent data from satellite observations[73]. The observational datasets used here are either the

only available data of the type (spatial and temporal coverage) we require or known high-quality data. Because long-term Arctic-wide precipitation, evaporation, total sea surface freshwater flux, and sea level pressure are not available from observations, we used reanalysis data and synthesized values from previous studies.

Data availability
The CMIP6 dataset is available at https://esgf-data.dkrz.de/search/cmip6-dkrz/. The data used to generate all figures are available at https://doi.org/10.5281/zenodo.14586011[74].

Code availability
The code used to generate all figures are available at https://doi.org/10.5281/zenodo.14586011[74].

References
1. Polyakov, I. et al. Greater role for Atlantic inflows on sea-ice loss in the Eurasian Basin of the Arctic Ocean. *Science* **356**, 285 (2017).
2. Sumata, H., de Steur, L., Divine, D. V., Granskog, M. A. & Gerland, S. Regime shift in Arctic Ocean sea ice thickness. *Nature* **615**, 443–449 (2023).
3. Proshutinsky, A. et al. Analysis of the Beaufort Gyre freshwater content in 2003-2018. *J. Geophys. Res. - Oceans* **124**, 9658–9689 (2019).
4. Shu, Q. et al. Arctic Ocean Amplification in a warming climate in CMIP6 models. *Sci. Adv.* **8**, eabn9755 (2022).
5. Proshutinsky, A. et al. Beaufort Gyre freshwater reservoir: State and variability from observations. *J. Geophys. Res. - Oceans* **114**, C00A10 (2009).
6. Aagaard, K., Coachman, L. K. & Carmack, E. On the halocline of the Arctic Ocean. *Deep Sea Res. Part A. Oceanograp. Res. Pap.* **28**, 529–545 (1981).
7. Peterson, B. J. et al. Trajectory shifts in the Arctic and Subarctic freshwater cycle. *Science* **313**, 1061–1066 (2006).
8. Serreze, M. C. et al. The large-scale freshwater cycle of the Arctic. *J. Geophys. Res. - Oceans* **111**, C11010 (2006).
9. Alkire, M. B. et al. A meteoric water budget for the Arctic Ocean. *J. Geophys. Res. - Oceans* **122**, 10020–10041 (2017).
10. Dong, J., Jin, M., Liu, Y. & Dong, C. Interannual variability of surface salinity and Ekman pumping in the Canada Basin during summertime of 2003–2017. *J. Geophys. Res.: Oceans* **126**, e2021JC017176 (2021).
11. Timmermans, M.-L. & Toole, J. M. The Arctic Ocean's Beaufort Gyre. *Annu. Rev. Mar. Sci.* **15**, 223–248 (2023).
12. Aagaard, K. & Carmack, E. C. The role of sea ice and other fresh-water in the Arctic circulation. *J. Geophys. Res.* **94**, 14485–14498 (1989).
13. Steele, M. et al. Circulation of summer Pacific halocline water in the Arctic Ocean. *J. Geophys. Res.: Oceans* **109**, C02027 (2004).
14. Woodgate, R. A., Aagaard, K., Swift, J. H., Falkner, K. K. & Smethie Jr, W. M. Pacific ventilation of the Arctic Ocean's lower halocline by upwelling and diapycnal mixing over the continental margin. *Geophys. Res. Lett.* **32**, L18609 (2005).
15. Timmermans, M.-L., Marshall, J., Proshutinsky, A. & Scott, J. Seasonally derived components of the Canada Basin halocline. *Geophys. Res. Lett.* **44**, 5008–5015 (2017).
16. Screen, J. A. & Simmonds, I. The central role of diminishing sea ice in recent Arctic temperature amplification. *Nature* **464**, 1334–1337 (2010).
17. Arzel, O., Fichefet, T., Goosse, H. & Dufresne, J.-L. Causes and impacts of changes in the Arctic freshwater budget during the 20th and 21st centuries in an AOGCM. *Clim. Dyn.* **30**, 37–58 (2008).
18. Zhang, J. et al. Labrador sea freshening linked to Beaufort Gyre freshwater release. *Nat. Commun.* **12**, 1229 (2021).
19. Weijer, W. et al. Interactions between the Arctic Mediterranean and the Atlantic Meridional Overturning Circulation: A review. *Oceanography* **35**, 118–127, (2022).
20. Haine, T. W. N., Siddiqui, A. H. & Jiang, W. Arctic freshwater impact on the Atlantic Meridional Overturning Circulation: status and prospects. *Philos. Trans. R. Soc. A: Math., Phys. Eng. Sci.* **381**, 20220185 (2023).
21. Armitage, T. et al. Arctic Ocean surface geostrophic circulation 2003–2014. *Cryosphere* **11**, 1767–1780 (2017).
22. Carmack, E. et al. Freshwater and its role in the Arctic Marine System: Sources, disposition, storage, export, and physical and biogeochemical consequences in the Arctic and global oceans. *J. Geophys. Res. Biogeosci.* **121**, 675–717 (2016).
23. Nishino, S. et al. Atlantic-origin water extension into the Pacific Arctic induced an anomalous biogeochemical event. *Nat. Commun.* **14**, 6235 (2023).
24. Armitage, T. et al. Arctic sea surface height variability and change from satellite radar altimetry and GRACE, 2003-2014. *J. Geophys. Res. - Oceans* **121**, 4303–4322 (2016).
25. Giles, K. A., Laxon, S. W., Ridout, A. L., Wingham, D. J. & Bacon, S. Western Arctic Ocean freshwater storage increased by wind-driven spin-up of the Beaufort Gyre. *Nat. Geosci.* **5**, 194–197 (2012).
26. Morison, J. et al. Changing Arctic Ocean freshwater pathways. *Nature* **481**, 66–70 (2012).
27. Rabe, B. et al. Arctic ocean basin liquid freshwater storage trend 1992-2012. *Geophys. Res. Lett.* **41**, 961–968 (2014).
28. Armitage, T. W. K., Manucharyan, G. E., Petty, A. A., Kwok, R. & Thompson, A. F. Enhanced eddy activity in the Beaufort Gyre in response to sea ice loss. *Nat. Commun.* **11**, 761 (2020).
29. Krishfield, R. A. et al. Deterioration of perennial sea ice in the Beaufort Gyre from 2003 to 2012 and its impact on the oceanic freshwater cycle. *J. Geophys. Res. Oceans* **119**, 1271–1305 (2014).
30. Proshutinsky, A., Dukhovskoy, D., Timmermans, M., Krishfield, R. & Bamber, J. Arctic circulation regimes. *Philos. Trans. R. Soc. A* **373**, 20140160 (2015).
31. Zhang, J. et al. The Beaufort Gyre intensification and stabilization: A model-observation synthesis. *J. Geophys. Res. - Oceans* **121**, 7933–7952 (2016).
32. Wang, Q. et al. Arctic sea ice decline significantly contributed to the unprecedented liquid freshwater accumulation in the Beaufort Gyre of the Arctic Ocean. *Geophys. Res. Lett.* **45**, 4956–4964 (2018).
33. Wang, Q. & Danilov, S. A synthesis of the upper Arctic Ocean circulation during 2000–2019: Understanding the roles of wind forcing and sea ice decline. *Front. Mar. Sci.* **9**, 863204 (2022).
34. Lin, P. et al. Recent state transition of the Arctic Ocean's Beaufort Gyre. *Nat. Geosci.* **16**, 485–491 (2023).
35. Wang, Q., Danilov, S. & Jung, T. Arctic freshwater anomaly transiting to the North Atlantic delayed within a buffer zone. *Nat. Geosci.* **17**, 1218–1221 (2024).
36. Zanowski, H., Jahn, A. & Holland, M. M. Arctic Ocean freshwater in CMIP6 ensembles: Declining sea ice, increasing ocean storage and export. *J. Geophys. Res.: Oceans* **126**, e2020JC016930 (2021).
37. Khosravi, N. et al. The Arctic Ocean in CMIP6 models: Biases and projected changes in temperature and salinity. *Earth's. Future* **10**, e2021EF002282 (2022).
38. Wang, S., Wang, Q., Wang, M., Lohmann, G. & Qiao, F. Arctic Ocean freshwater in CMIP6 coupled models. *Earth's. Future* **10**, e2022EF002878 (2022).
39. Muilwijk, M. et al. Divergence in climate model projections of future Arctic Atlantification. *J. Clim.* 1–53 (2023).
40. Ilicak, M. et al. An assessment of the Arctic Ocean in a suite of interannual CORE-II simulations. Part III: Hydrography and fluxes. *Ocean Model.* **100**, 141–161 (2016).
41. Shu, Q. et al. Arctic ocean simulations in the CMIP6 Ocean Model Intercomparison Project (OMIP). *Geosci. Model Dev.* **16**, 2539–2563 (2023).

42. Wang, Q., Wekerle, C., Danilov, S., Wang, X. & Jung, T. A 4.5 km resolution Arctic Ocean simulation with the global multi-resolution model FESOM 1.4. *Geosci. Model Dev.* **11**, 1229–1255 (2018).

43. Wang, Q. et al. Impact of increased resolution on Arctic Ocean simulations in Ocean Model Intercomparison Project phase 2 (OMIP-2). *Geosci. Model Dev.* **17**, 347–379 (2024).

44. Steele, M., Morley, R. & Ermold, W. Phc: A global ocean hydrography with a high quality Arctic Ocean. *J. Clim.* **14**, 2079–2087 (2001).

45. Landerer, F. W., Jungclaus, J. H. & Marotzke, J. Ocean bottom pressure changes lead to a decreasing length-of-day in a warming climate. *Geophys. Res. Lett.* **34**, L06307 (2007).

46. Dangendorf, S. et al. Data-driven reconstruction reveals large-scale ocean circulation control on coastal sea level. *Nat. Clim. Change* **11**, 514–520 (2021).

47. Wang, Q. Stronger variability in the Arctic Ocean induced by sea ice decline in a warming climate: Freshwater storage, dynamic sea level and surface circulation. *J. Geophys. Res.-Oceans* **126**, e2020JC016886 (2021).

48. Manucharyan, G. & Spall, M. Wind-driven freshwater buildup and release in the Beaufort Gyre constrained by mesoscale eddies. *Geophys. Res. Lett.* **43**, 273–282 (2016).

49. Meneghello, G., Marshall, J., Cole, S. & Timmermans, M. L. Observational inferences of lateral eddy diffusivity in the halocline of the Beaufort Gyre. *Geophys. Res. Lett.* **44**, 12331–12338 (2017).

50. Li, X. et al. Eddy activity in the Arctic Ocean projected to surge in a warming world. *Nat. Clim. Change* **14**, 156–162 (2024).

51. Zhang, X. et al. Arctic cyclones have become more intense and longer-lived over the past seven decades. *Commun. Earth Environ.* **4**, 348 (2023).

52. Parker, C. L., Mooney, P. A., Webster, M. A. & Boisvert, L. N. The influence of recent and future climate change on spring Arctic cyclones. *Nat. Commun.* **13**, 6514 (2022).

53. Moore, G. W. K., Schweiger, A., Zhang, J. & Steele, M. Collapse of the 2017 winter Beaufort High: A response to thinning sea ice? *Geophys. Res. Lett.* **45**, 2860–2869 (2018).

54. Kenigson, J. S. & Timmermans, M.-L. Arctic cyclone activity and the Beaufort High. *J. Clim.* **34**, 4119–4127 (2021).

55. Rantanen, M. et al. The Arctic has warmed nearly four times faster than the globe since 1979. *Commun. Earth Environ.* **3**, 168 (2022).

56. Vavrus, S. J. & Alkama, R. Future trends of Arctic surface wind speeds and their relationship with sea ice in CMIP5 climate model simulations. *Clim. Dyn.* **59**, 1833–1848 (2022).

57. Zapponini, M. & Goessling, H. F. Atmospheric destabilization leads to Arctic Ocean winter surface wind intensification. *Commun. Earth Environ.* **5**, 262 (2024).

58. Wang, S. et al. Nonmonotonic change of the Arctic Ocean freshwater storage capability in a warming climate. *Geophys. Res. Lett.* **48**, e2020GL090951 (2021).

59. Heuzé, C., Zanowski, H., Karam, S. & Muilwijk, M. The deep Arctic Ocean and Fram Strait in CMIP6 models. *J. Clim.* 1–68 (2023).

60. O'Neill, B. C. et al. The Scenario Model Intercomparison Project (ScenarioMIP) for CMIP6. *Geosci. Model Dev.* **9**, 3461–3482 (2016).

61. Brunner, L. et al. Reduced global warming from CMIP6 projections when weighting models by performance and independence. *Earth Syst. Dyn.* **11**, 995–1012 (2020).

62. Danilov, S., Sidorenko, D., Wang, Q. & Jung, T. The Finite-volumE Sea ice–Ocean Model (FESOM2). *Geosci. Model Dev.* **10**, 765–789 (2017).

63. Scholz, P. et al. Assessment of the Finite-volumE Sea ice-Ocean Model (FESOM2.0) – part 1: Description of selected key model elements and comparison to its predecessor version. *Geosci. Model Dev.* **12**, 4875–4899 (2019).

64. Shu, Q., Qiao, F., Liu, J., Bao, Y. & Song, Z. Description of FIO-ESM version 2.1 and evaluation of its sea ice simulations. *Ocean Model.* **187**, 102308 (2024).

65. Bao, Y., Song, Z. & Qiao, F. FIO-ESM version 2.0: Model description and evaluation. *J. Geophys. Res.: Oceans* **125**, e2019JC016036 (2020).

66. Zhang, M.-Z., Xu, Z., Han, Y. & Guo, W. Evaluation of CMIP6 models toward dynamical downscaling over 14 CORDEX domains. *Clim. Dyn.* **62**, 4475–4489 (2022).

67. Tsujino, H. et al. JRA-55 based surface dataset for driving ocean–sea-ice models (JRA55-do). *Ocean Modell.* **130**, 79–139 (2018).

68. Polyakov, I. V., Pnyushkov, A. V. & Carmack, E. C. Stability of the Arctic halocline: a new indicator of arctic climate change. *Environ. Res. Lett.* **13**, 125008 (2018).

69. Dai, A., Qian, T., Trenberth, K. E. & Milliman, J. D. Changes in continental freshwater discharge from 1948 to 2004. *J. Clim.* **22**, 2773–2792 (2009).

70. Dee, D. P. et al. The ERA-Interim reanalysis: configuration and performance of the data assimilation system. *Q. J. R. Meteorol. Soc.* **137**, 553–597 (2011).

71. Hersbach, H. et al. The ERA5 global reanalysis. *Q. J. R. Meteorol. Soc.* **146**, 1999–2049 (2020).

72. Gelaro, R. et al. The modern-era retrospective analysis for research and applications, version 2 (MERRA-2). *J. Clim.* **30**, 5419–5454 (2017).

73. Fetterer, F., Knowles, K., Meier, W., Savoie, M. & Windnage, A. K. Sea Ice Index, Version 3. Boulder, Colorado USA. NSIDC: National Snow and Ice Data Center. updated daily (2017).

74. Shu, Q. Code and data for the paper "Dominant inflation of the Arctic Ocean's Beaufort Gyre in a warming climate". *Zenodo* https://doi.org/10.5281/zenodo.14586011 (2024).

Author contributions
Q.W. and Q.S. conceived the study. Q.W. wrote the first paper draft. Q.S. performed the FESOM2 simulations. SW analyzed the CMIP data. Q.S., X.L. and Q.W. analyzed the FESOM2 data. S.D., F.Q., Z.S., F.W. and T.J. contributed to interpreting model results and improving the article.

Competing interests
The authors declare no competing interests.

Additional information
Supplementary information The online version contains supplementary material available at https://doi.org/10.1038/s43247-025-02028-3.

Correspondence and requests for materials should be addressed to Qiang Wang.

Peer review information *Communications Earth & Environment* thanks the anonymous reviewers for their contribution to the peer review of this work. Primary Handling Editor: Alireza Bahadori. A peer review file is available

Reprints and permissions information is available at http://www.nature.com/reprints